Journal of Materials Chemistry A

PAPER

View Article Online
View Journal | View Issue

Cite this: J. Mater. Chem. A, 2016, 4, 9858

Bulky crystalline $BiVO_4$ thin films for efficient solar water splitting

Miao Zhong,[ab] Takashi Hisatomi,[ab] Tsutomu Minegishi,[ab] Hiroshi Nishiyama,[ab] Masao Katayama,[ab] Taro Yamada[ab] and Kazunari Domen*[ab]

Received 14th April 2016
Accepted 25th May 2016

DOI: 10.1039/c6ta03072f

www.rsc.org/MaterialsA

We report a new fabrication method of flat, uniform $BiVO_4$ films on an electrically conductive transparent indium tin oxide (ITO) film based on a solution process for depositing bismuth precursor films and a high-temperature calcination process with an organic vanadium precursor. The synthesised $BiVO_4$ films, composed as a monolayer of crystallites (diameter $\leq$ 1 μm) fixed on the ITO, realised half-cell solar-to-hydrogen energy conversion efficiencies of over 1.5% by the aid of impregnated CoO_x and atomic-layer-deposited NiO when tested as oxygen-evolving photoanodes for water splitting under solar simulator AM 1.5G illumination. Stoichiometric oxygen and hydrogen were generated with Faraday efficiencies of unity over 12 h at 0.6–0.9 V_{RHE}. This morphology of our bulky semi-transparent $BiVO_4$ films exhibited state-of-the-art solar water splitting performances.

Introduction

Photoelectrochemical (PEC) water splitting — harvesting solar energy to produce clean and renewable hydrogen fuels from water — is a promising technique to fulfil the increasing energy demands of modern society with minimum environmental impacts.[1–3] Considerable efforts have been made to realize high-performance and low-cost PEC overall water splitting devices. In PEC hydrogen evolution reactions (HERs), high solar energy conversion efficiencies are achieved when p-type semiconductors that are excellent light absorbers with high carrier mobility are used in photocathode-based half-cell PEC devices.[2,4] However, the development of efficient and stable photoanodes for oxygen evolution reactions (OERs) is still a challenging field.

One essential problem that impedes photoanode efficiency is the high activation energy associated with the complex four-electron OER process.[5] Holes easily recombine at photoanode/electrolyte interfaces before they oxidise water. Earth-abundant CoPi[6] and Ni/Fe layered-double-hydroxide (LDH)[7,8] have been developed as robust catalysts to largely improve OER kinetics in bias-driven PEC electrolysis. Besides the decoration of effective OER catalysts, suppression of charge recombination at photoanode surfaces by conformal coating of p-type materials has been reported.[8,9] In this way, dangling bonds at photoanode surfaces are passivated and buried p/n junctions are created to increase the hole lifetime.

Suppression of charge recombination in the photoanode bulk is another fundamental aspect for improving PEC performances. Photoanode materials that can effectively separate charges and efficiently transport holes are required. $BiVO_4$ is one of the most attractive candidates,[10–12] due to its deep valence band for OER under visible light and long-term stability in near-neutral aqueous solutions. Further, $BiVO_4$ has a long carrier lifetime of ~40 ns compared to that of <10 ps for other oxide photocatalysts such as hemitate.[13,14] However, the carrier mobility in $BiVO_4$ is low at ~0.044 $cm^2\ V^{-1}\ s^{-1}$, indicating that most of the photo-generated holes are localised in $BiVO_4$.

To achieve efficient charge separation in $BiVO_4$, attempts have been made on fabricating (1) monolayer $BiVO_4$ sub-micro nanoparticles on conducting Ti metal by particle transfer methods,[8] (2) $BiVO_4$ homo-/hetero-junctions such as $BiVO_4$/WO_3/ITO films[10,14] and (3) nanostructures such as nanowire arrays.[15,16] Recently, Choi *et al.* reported nanoporous $BiVO_4$ with state-of-the-art photocurrent density and efficiency.[12] A simple and effective electrodeposition–annealing process was applied for synthesizing nanoporous $BiVO_4$ with particle sizes of ~80 nm. Nanostructures drastically improve charge separation and surface areas for largely enhanced PEC performances.

However, nanostructures have disadvantages that warrant special care with respect to their practical applications. (1) Their mechanical strength is not satisfactory and achieving mechanical robustness is a stubborn challenge for practical operation. It is difficult to improve the mechanical strength of certain materials, especially nanostructured materials. (2) Coating of other functional materials over entire nanostructures is also difficult compared to that for flat thin films. This further hampers the construction of tandem devices when starting with nanostructures.

[a]Department of Chemical Systems Engineering, The University of Tokyo, 7-3-1 Hongo, Bunkyo-ku, Tokyo 113-8656, Japan. E-mail: domen@chemsys.t.u-tokyo.ac.jp
[b]Japan Technological Research Association of Artificial Photosynthetic Chemical Process, 2-11-9 Iwamotocho, Chiyoda-ku, Tokyo 101-0032, Japan

In contrast, multi-layered tandem film devices with anti-reflective coatings are commercialised for solar cells. Thus also for PEC applications aiming for future industrialisation, it is desirable to fabricate robust and flat $BiVO_4$ thin films with exact stoichiometry, the most photoactive crystallographic structure, and high crystallinity with the particle size optimised.

In this study, we present an anodic electrodeposition and calcination process for fabricating bulky $BiVO_4$ crystalline films on transparent ITO glass for use as photoanodes in solar water splitting cells. The fabricated films were proven to be mechanically robust. After surface decoration with CoO_x catalysts and conformal deposition of NiO layers, a half-cell solar-to-hydrogen (HC-STH) conversion efficiency of over 1.5% was realised. Stoichiometric hydrogen and oxygen were generated with unity Faraday efficiency over 12 h.

Experimental

Deposition of Bi precursor thin films

First, 25 mL 0.1 M $Bi(NO_3)_3$ in acetic acid was prepared. The pH of the prepared solution was adjusted to 4.8 by adding 5 M NaOH aqueous solution. Then 20 mL 0.3 M *p*-benzoquinone in ethanol (99.95%) was added into the solution. After gently stirring for 1 h, the colour of the solution changed to transparent dark brown. Electrodeposition in this mixture was performed on ITO glass plates (Geomatec, sheet resistivity ~ 5 Ω sq^{-1}, 30 mm × 10–30 mm × 1 mm thickness). A potentiostat (Hokuto Denko, HSV-100) was used at room temperature with ITO glass as the working electrode, an Ag/AgCl reference electrode and a Pt counter electrode. The ITO working electrode was maintained at 2.3 $V_{Ag/AgCl}$. The optimised deposition time was 7 min.

Synthesis of $BiVO_4$ thin films

The Bi precursor film was drop-painted with a 1 : 1 dimethyl sulfoxide/ethanol solution of vanadyl diacetylacetonate ($VO(acac)_2$, 0.2 M). The casting amount was 0.075 mL for a 20 mm × 20 mm Bi precursor film. The $VO(acac)_2$/Bi precursor film was

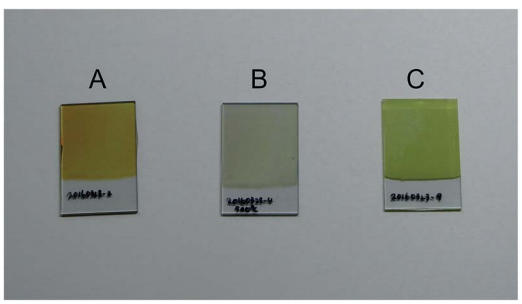

Fig. 1 Sample Bi precursor films and $BiVO_4$ films on ITO glass. (A) Bi precursor film after the deposition of BiC_xO_y. The initial BiC_xO_y was deposited in 25 mL 0.1 M $Bi(NO_3)_3$/CH_3COOH + 20 mL 0.3 M *p*-benzoquinone/C_2H_5OH (pH adjusted at 5.3) at 2.3 $V_{Ag/AgCl}$ for 7 min. (B) BiC_xO_y heated at 500 °C in air (temperature ramped up to 500 °C with a heating rate of 2 °C min^{-1} and then cooled down naturally). (C) $BiVO_4$ films prepared by calcining as-deposited BiC_xO_y with 0.5 mM $VO(acac)_2$/1 : 1 ethanol + DMSO for 1 hour in air. The substrate pieces of glass were all 20 mm × 30 mm in size.

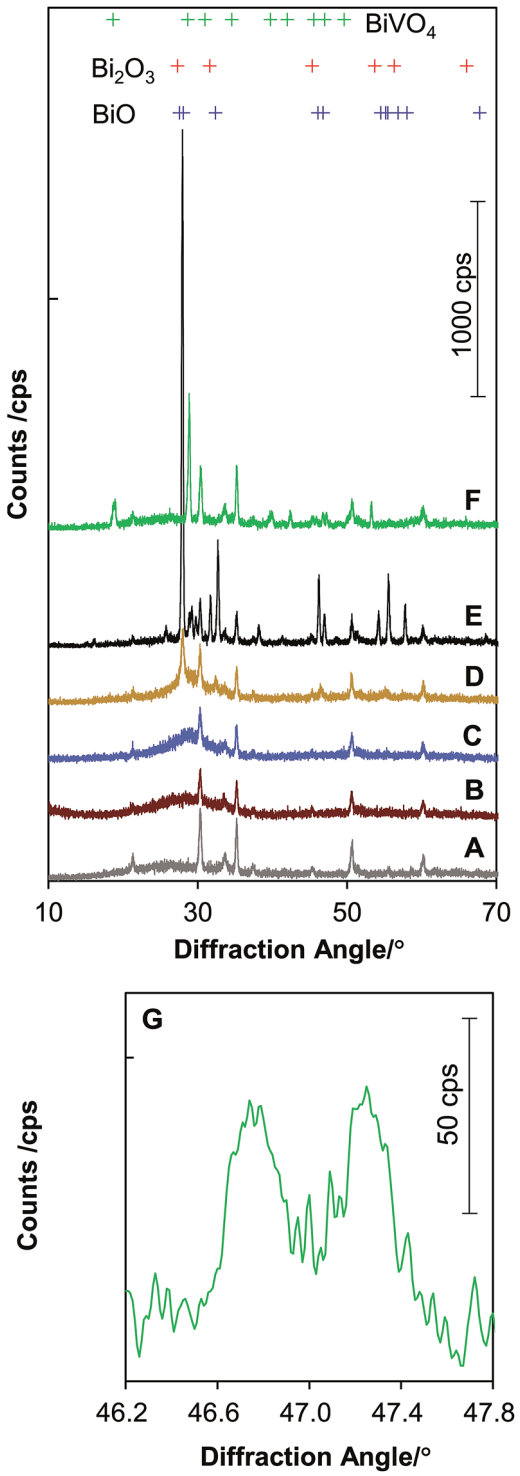

Fig. 2 X-ray diffraction spectra of (A) a bare ITO glass piece (Geomatec, ITO thickness ~ 500 nm, sheet resistivity ~ 5 Ω sq^{-1}), (B) the as-deposited BiC_xO_y, (C) BiC_xO_y heated at 180 °C in air, (D) at 300 °C, (E) at 500 °C, (F) $BiVO_4$ film by calcination of as-deposited BiC_xO_y, and $VO(acac)_2$ at 520 °C for 1 h, (G) an expanded spectrum from curve (F) for (024) and (204) diffractions of the scheelite monoclinic $BiVO_4$. The X-ray wavelength was 0.15418 nm (Cu Kα). The standard diffraction peak positions are indicated by + at the top, referring to ref. 25 for BiO, ref. 26 for Bi_2O_3 and ref. 27 for $BiVO_4$.

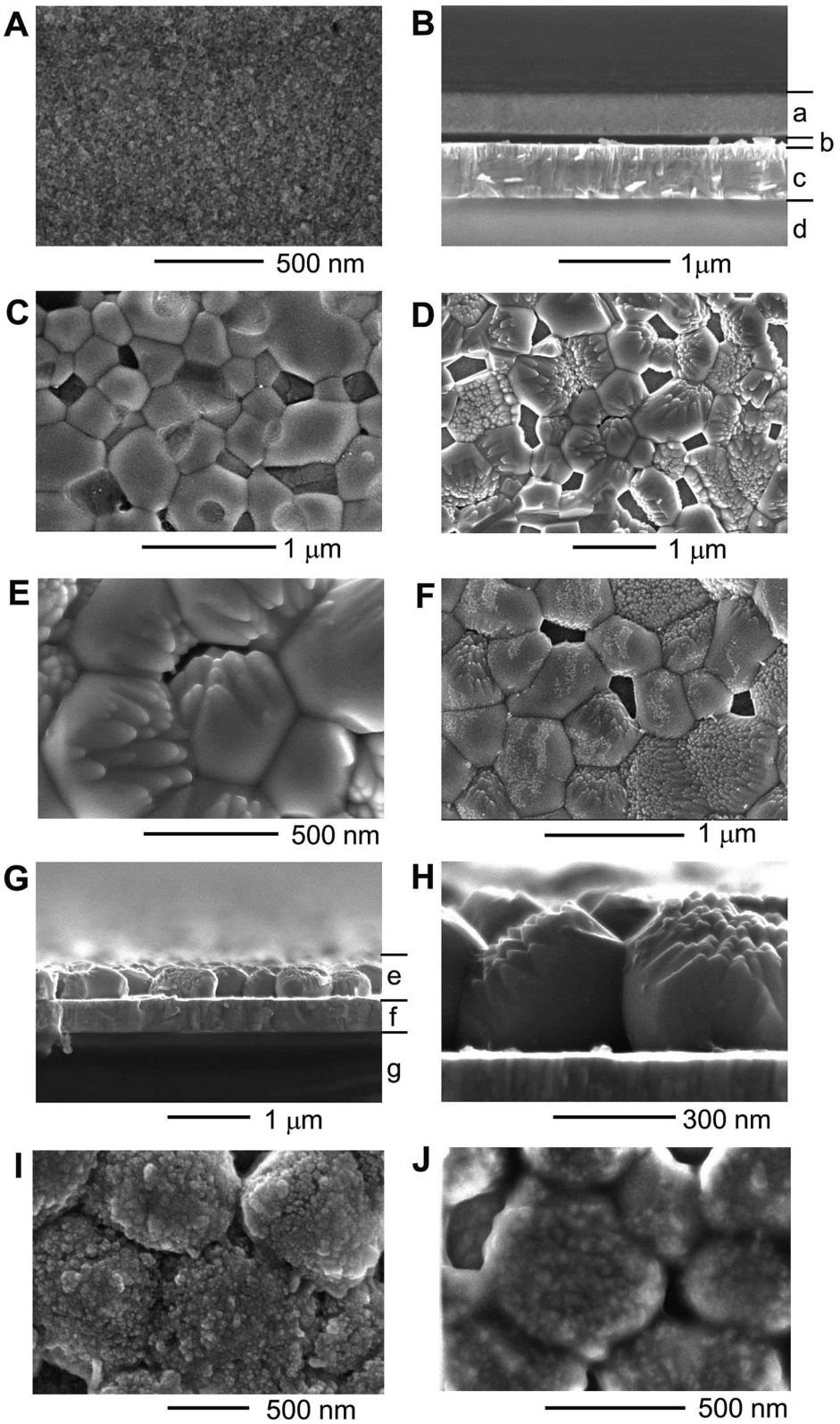

Fig. 3 SEM images of precursors and completed $BiVO_4$ films. (A) Top view of as-deposited BiC_xO_y. (B) The cross section of as-deposited BiC_xO_y. On the right of this image, (a) BiC_xO_y, (b) a gap accidentally made when clamping this sample, (c) ITO, (d) glass. (C) Top view of BiC_xO_y heated at 500 °C. (D) Top view of the $BiVO_4$ film by calcination of as-deposited BiC_xO_y, and $VO(acac)_2$ at 520 °C for 1 hour. Rinsed in 1 M NaOH. (E) A magnification of the central part of (D). (F) Top view of the $BiVO_4$ film by calcination of BiC_xO_y, pre-heated at 500 °C (equivalent to image C) and then with $VO(acac)_2$ at 520 °C for 1 h. Rinsed in 1 M NaOH. (G and H) Cross sections of the final $BiVO_4$ film (equivalent to image D), (e) $BiVO_4$, (f) ITO, (g) glass. (I) Top view of a $BiVO_4$ film modified by impregnation of CoO_x and ALD of NiO. (J) $NiO/CoO_x/BiVO_4$ photoelectrode after PEC performance test at 0.6 V_{RHE} for 48 hours.

calcined in a muffle furnace in air at various temperatures from 490–530 °C. The excess amount of VO_x was washed away in 1 M NaOH solution for 10 min with gentle stirring. The obtained $BiVO_4$ films were then cleaned with DI water and dried at room temperature. In our experiments, $BiVO_4$ films synthesised at 520 °C for 2 h with the initial temperature ramping rate of 2 °C min^{-1} exhibited the best performance.

Loading of CoO_x on $BiVO_4$

The $BiVO_4$ films were immersed in a 20 mL 0.01 M $Co(NO_3)_2$ and 0.01 M NH_3 H_2O solution at pH 8.4 for 0.5 h. Then the films were washed with DI water and annealed in air at 250 °C for 0.5 h.

Atomic-layer deposition of NiO on $CoO_x/BiVO_4$

Atomic-layer deposition (ALD) was applied to deposit NiO on the $CoO_x/BiVO_4$ films. Bis-(2,2,6,6-tetramethylheptane-3,5-dionato) nickel(II) ($Ni(thd)_2$ in short) and H_2O were used as the precursors. $Ni(thd)_2$ was heated to 165 °C and H_2O was set to 15 °C. The temperature in the deposition chamber was 260 °C. One ALD cycle consists of an H_2O pulse for 6 s, N_2 purging for 3 s, pressurising the $Ni(thd)_2$ container by N_2 gas (500 sccm) for 3 s, a $Ni(thd)_2/N_2$ pulse for 6 s, and a N_2 purging for 3 s. Before ALD, $CoO_x/BiVO_4$ was treated in an ozone plasma cleaning machine for 5 min to increase surface wettability with respect to hydroxyl ions. For $BiVO_4$ films, 300 cycles ALD delivered the best performances. Excess deposition of NiO on $CoO_x/BiVO_4$ could be thinned by 50 mV s^{-1} cyclic-voltammetry scans from −0.6 to 0.8 $V_{Ag/AgCl}$ in a 1 M pH 6 Na_2SO_4 solution.

Characterizations

Scanning electron microscopic (SEM) observations were carried out using a Hitachi SU8020 system. The X-ray diffraction (XRD) was measured by a SmartLab XRD (Rigaku, Japan). The X-ray wavelength was 0.15418 nm (Cu Kα).

The PEC performances were investigated using a three-electrode electrochemical configuration in a 0.5 M potassium borate (K_3BO_3) buffer solution at pH = 9.5 by a solar simulator light source (SAN-EI electronic, XES40S1). The light intensity of this solar simulator was adjusted to AM 1.5G (100 mW cm^{-2}) by measuring with a calibrated photometer (Hamamatsu model S2281). The electrolyte was stirred and bubbled with Ar gas before and during measurements. An Ag/AgCl electrode in saturated KCl solution was used as a reference electrode and a Pt coil was used as the counter electrode. The potential unit is converted to the reversible hydrogen electrode according to the Nernst equation,

$$V_{RHE} = V_{Ag/AgCl} + 0.059pH + V^0_{Ag/AgCl}$$

$$V^0_{Ag/AgCl} = 0.199 \text{ V at } 25\ ^\circ C$$

The incident light spectral analysis for the photocurrent was performed using a Xe lamp (Asahi Spectra, MAX-302) equipped with bandpass filters (central wavelengths: 400–540 nm, every 20 nm; full width at half maximum: 10 nm). The irradiance spectra of the light incident on the electrode surface were measured with a spectroradiometer (EKO Instruments, LS-100, absolutely calibrated for the intensity).

The gas chromatographic (GC) quantification of H_2 and O_2 during the PEC H_2O splitting was performed with a dedicated setup. An air-tight three-electrode PEC cell with $NiO/CoO_x/BiVO_4$ working electrodes, Ag/AgCl reference electrodes and Cr-coated Pt counter electrodes was used for GC analyses. Here, Cr was coated on Pt wire to suppress the reverse reaction of oxygen reduction on the Pt wire in solution. The PEC cell was connected to a vacuum pump and a micro GC (Inficon Co., Ltd, 3000). Before measurement, the PEC cell was pumped to a low vacuum and then purged with Ar sufficiently to get rid of N_2 and O_2 gases in the PEC cell. H_2 and O_2 evolution were measured in 0.5 M K_3BO_3 buffer solution at pH 9.5 under simulated sunlight illumination for 12 h with potential *vs.* RHE at 0.6 and 0.9 V_{RHE}. The electric current passing through the outer circuit was recorded by a potentiostat (Princeton Research, VersaSTAT 3000) during H_2 and O_2 evolution reactions. The GC peak areas for H_2 and O_2 were converted to μmol using calibration curves, obtained by measuring the same amounts of H_2 and O_2 gases pre-injected in the PEC cell. The sampling of the gas in the PEC cell for GC was performed every 20 min.

Results and discussion

Fig. 1 shows photographs of ITO glass plates covered by an as-deposited Bi precursor film, a Bi precursor film annealed at 500 °C, and the $BiVO_4$ film prepared according to the above-mentioned procedures. We temporarily call the precursor film BiC_xO_y. The as-deposited BiC_xO_y film might be hydrated and contain carbonate and other carbonaceous components. Bubbles were seen when this film was immersed in dilute HCl, and the gas was probably CO_2. During the electrochemical deposition process, CH_3COO^- in pH 5–6 solution can be altered into CO_3^{2-} by Kolbe electrolysis. The mechanism of Bi accumulation on this positively polarised electrode must include elementary reactions involving CH_3COO^-, which is the major component of this solution.

Annealing the BiC_xO_y film in a muffle furnace in air altered the colour of the film. Before annealing, the as-deposited BiC_xO_y film looks brown (Fig. 1A), and after annealing at 500 °C the colour is close to white (Fig. 1B). The change in colour is related to the changes in the Bi compounds in the film. XRD spectra were recorded for the films from as-deposited BiC_xO_y and annealed BiC_xO_y, shown in Fig. 2B–E. The spectra always contain diffractions from the substrate ITO (A). The as-deposited BiC_xO_y and annealed samples below 300 °C exhibit broad scattering at 28° of the diffraction angle (Fig. 2B). The films were amorphous, probably composed of nano-crystallites of Bi carbonaceous compounds. The components of BiC_xO_y might be those such as bismuth carbonate, bismuth hydroxide carbonate[18,19] and other carbonaceous materials. Above the annealing temperature of 300 °C, XRD exhibited sharp peaks (Fig. 2D and E), better matching the standard peak positions of crystalline BiO than those of Bi_2O_3 (Fig. 2 top). We carried out

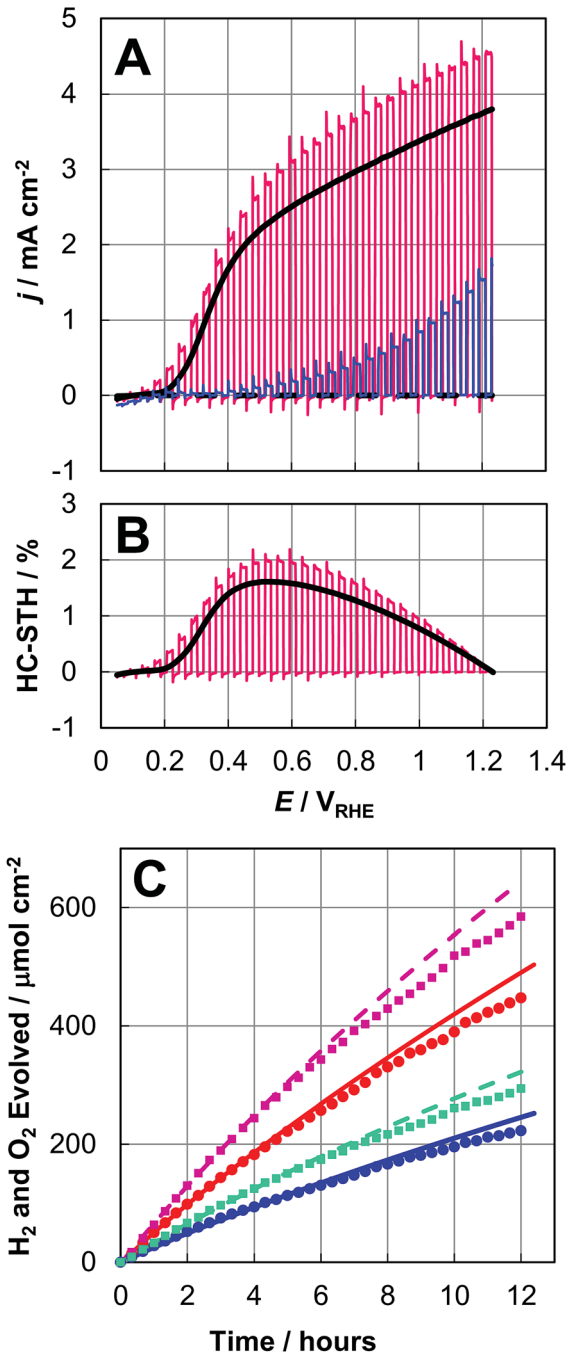

Fig. 4 The photoelectrochemical (PEC) performance tests for the bare $BiVO_4$ and $NiO/CoO_x/BiVO_4$ photoelectrodes by AM 1.5G solar simulator excitation in a 0.5 M K_3BO_3 solution adjusted to pH 9.5. (A) The photocurrent density (j/mA cm^{-2}) as a function of the electrode potential (E/V_{RHE}). Blue curve: by PEC measurement with chopped light for a bare $BiVO_4$ electrode. Red curve: our best-performance $NiO/CoO_x/BiVO_4$ electrode with an active surface area of 0.95 cm^2. Black bold line: average curve for 10 new different $NiO/CoO_x/BiVO_4$ electrodes. Broken black line: average dark currents for the same samples, (B) the half-cell solar-to-hydrogen (HC-STH) conversion efficiency. (C) Time course of H_2 and O_2 evolution with at $E = 0.6$ V_{RHE} and $E = 0.9$ V_{RHE} for 12 h. The colour codes are: red – H_2, 0.6 V_{RHE}, blue – O_2, 0.6 V_{RHE}, purple – H_2, 0.9 V_{RHE}, green – O_2, 0.9 V_{RHE}.

elemental analysis of the as-deposited BiC_xO_y film and BiC_xO_y film annealed at 500 °C, having scratched them off from the ITO glass. This powder was subjected to decomposition in HNO_3 and Bi quantification by means of inductively coupled plasma (ICP) spectroscopy. The Bi contents for as-deposited BiC_xO_y film and BiC_xO_y film annealed at 500 °C were 76.8% w/w and 86.4% w/w, respectively.

The annealed film is compositionally close to BiO (Bi 92.9% w/w) or Bi_2O_3 (Bi 89.7% w/w). Although there were some residual carbonaceous materials therein, the films annealed at 500 °C were determined to be mainly composed of crystalline BiO.

The morphological change of BiC_xO_y upon annealing is visualised by scanning electron microscopy, as shown in Fig. 3. The original as-deposited BiC_xO_y comprised a flat, smooth, homogeneous layer with a thickness of ~300 nm (Fig. 3A and B). The top view indicates that the film consists of fine grains (diameter < 10 nm). As annealing temperature was raised and reached 500 °C, the grain size increased up to 1 μm (Fig. 3C). The grains compose a monolayer over the ITO surface and some voids are seen surrounded by grains. This bulky morphology of BiO particles is the prototype of $BiVO_4$ films, as discussed later.

Calcination of the as-deposited BiC_xO_y with vanadyl bis-acetylacetonate ($VO(acac)_2$) at 520 °C formed highly crystalline $BiVO_4$ of scheelite monoclinic type, as seen in the XRD spectra in Fig. 2F and G. Splitting of the $BiVO_4$ (024) and (204) peaks at 46.7° and 47.3° (Fig. 2B) was clearly observed. This is essentially different from the single (024) peak of ~47° for tetragonal $BiVO_4$.[21] Note that there is no ITO peak between 46° and 48°, which rules out the other possibility for this XRD peak splitting.

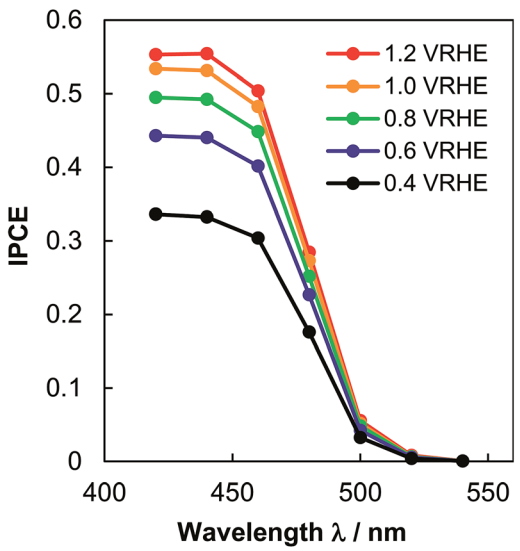

Fig. 5 The wavelength dependence of incident photon conversion efficiency (IPCE) of a $NiO/CoO_x/BiVO_4$ photoelectrode of the average performance in a 0.5 M K_3BO_3 solution at pH 9.5. The photocurrent was recorded within 10 min after starting chronoamperometric measurement, using the bandpass-filtered Xe lamp. The IPCE values are calculated by $\mathrm{IPCE} = \frac{j(\lambda)/e}{P(\lambda)/(hc/\lambda)}$ where λ: monochromatic light wavelength/nm, $j(\lambda)$: current density/mA cm^{-2}, $P(\lambda)$: light power density/mW cm^{-2}, e: electron charge = 1.60×10^{-19} C, h: Plank constant = 6.63×10^{-34} J s, and c: light speed = 3.00×10^{8} m s^{-1}.

$BiVO_4$ films calcined at different temperatures between 490 °C and 530 °C were all of the same monoclinic structure. The synthesised $BiVO_4$ is made of large $BiVO_4$ particles with an in-plane diameter of ~1 μm and a thickness of ~300 nm (Fig. 3D and E). Some grains, probably depending upon the crystallographic orientation, have a bunch of needle-like shapes aligned along one direction.

It is notable that the final $BiVO_4$ particles (Fig. 3D and E) look quite similar in size and in shape to the BiO particles formed by annealing at 500 °C (Fig. 3C). Actually BiC_xO_y pre-annealed at 500 °C was subjected to calcination with $VO(acac)_2$ at 520 °C. The same shape of $BiVO_4$ crystallites (Fig. 3F) appeared as seen in Fig. 3D and E. Presumably the temperature ramping of BiC_xO_y + $VO(acac)_2$ from room temperature induces the formation of BiO crystallites near 500 °C, and the BiO crystallites are converted into $BiVO_4$ crystallites simultaneously with diffusion of V.[17–20]

The $BiVO_4$ crystallites formed a particle monolayer firmly fixed on ITO. The in-plane diameter of $BiVO_4$ crystallites is larger than that of the previously reported $BiVO_4$ nanostructures or films synthesised by spray pyrolysis,[11] electrochemical processes,[12] chemical vapour deposition[22] or co-evaporation.[23]

The two-step synthesis of $BiVO_4$ was first reported by Choi and co-workers using BiOI as a starting material.[12] The key step in their synthesis is the fabrication of very thin BiOI nanosheets that have a large surface area to make the Bi and V precursors be sufficiently in contact with each other for uniform $BiVO_4$ nucleation during calcination. Differently from their BiOI cathodic deposition, we fabricated a dense Bi precursor film on ITO as anodes. The Bi precursor film is advantageous for the fabrication of bulky crystalline $BiVO_4$ films, evidenced by the conversion from BiO crystallites observed by XRD and SEM analyses as described above.

The present $BiVO_4$ films were mechanically robust. The film never came off even when subjected to pressing, rubbing or scratching by a finger or wiping with tissue paper. More systematically, we performed a peeling-off test with adhesive tape. A piece of adhesive tape ("mending tape") was applied on the films, and pressed by loading a weight over the tape at 220 g cm^{-2} for 1 min. Then the tape was peeled off and the glue surface of the tape was inspected. In the case of present $BiVO_4$ films, nothing looked transferred to the adhesive. The nanoporous films we reproduced according to the recipe[12] did not survive these tests and released $BiVO_4$ dust. This demonstrates the high reliability of this $BiVO_4$ crystalline monolayer towards usage under mechanically severe conditions, such as in a flow of electrolytic solutions or in repetitive heating/cooling cycles.

As for the O_2-evolution cocatalysts, CoO_x was loaded on $BiVO_4$ films by impregnation, and atomic layer deposition (ALD) was performed to deposit NiO on the surface of CoO_x-loaded $BiVO_4$. After PEC measurement, NiOOH was formed on the top surfaces of NiO nanoparticles (Fig. 3J). This state of the NiOOH are supposed to contain a large amount of surface hydroxyl ions for efficient OERs.[7,8] Ultrathin NiOOH can allow penetration of hydroxyl ions and also enable hydroxyl ions to be in contact with the buried CoO_x for a dual OER catalyst effect.[7,8,12] A small amount of Co incorporation in NiOOH can also possibly increase its electric conductivity to reduce applied potential loss within the NiOOH layer, for realising high PEC performances.[7,12,24]

The PEC performance of the bare $BiVO_4$ and $NiO/CoO_x/BiVO_4$ photoanodes was measured in 0.5 M pH 9.5 potassium borate (K_3BO_3) buffer solutions under simulated air mass (AM) 1.5G illumination. Fig. 4A shows the photocurrent density (j) as a function of the electrode potential (E). The chopped light blue and red j–E curves represent the PEC performances of our bare $BiVO_4$ electrode and our best $NiO/CoO_x/BiVO_4$ electrode, respectively. The best electrode had a light acceptance/electrolytically active area of 0.95 cm^2. The black j–E curve is an average PEC performance from j–E curves obtained with 10 different $NiO/CoO_x/BiVO_4$ test samples, with the average dark current also shown. We take this average data as the representative characteristics of the present $NiO/CoO_x/BiVO_4$ photoanode. The photocurrent onset potential was ~0.2 V_{RHE} in Fig. 4A. The anodic photocurrent at this low applied-bias region indicates the effective separation of photogenerated charges and efficient migration of holes towards $BiVO_4$ surfaces for OERs. The photocurrent density is over 2.5 mA cm^{-2} at 0.6 V_{RHE} for the $NiO/CoO_x/BiVO_4$ photoanode. The HC-STH curves, shown in Fig. 4B, are calculated from the j–E curves by

$$\text{HC-STH} = (1.23E/V_{RHE})j/(\text{solar simulator power/W cm}^{-2})$$

The average HC-STH curve reaches the maximum of 1.5% at 0.56 V_{RHE}, which was markedly high among the reported single-photon photoanodes. This high performance of the semi-transparent $BiVO_4$ films is suitable for the construction of parallel electrode devices, such as integrated solar water splitting devices with a narrow-bandgap photocathode or photovoltaic cells placed behind $BiVO_4$/ITO/glass to utilize the transmitted solar photons through this semi-transparent electrode.

To confirm HERs at the Pt electrode and OERs at the $NiO/CoO_x/BiVO_4$ photoanode, the evolved gas was analysed by gas chromatography. The plots in Fig. 4C indicate the amounts of accumulated H_2 and O_2 gases within the PEC reactor measured by gas chromatography. The curves are obtained by integrating the photocurrent density as a function of time and converted into the accumulated amounts of H_2 and O_2 under the assumption that the photocurrent was completely consumed at the Pt cathode with 2 electrons for one H_2 molecule and at the $BiVO_4$ photoanode with 4 electrons for one O_2 molecule. The $NiO/CoO_x/BiVO_4$ photoanodes were held at constant potentials of 0.6 and 0.9 V_{RHE} in three-electrode configurations for 12 h. The evolution of H_2 and O_2 with a ratio of 2 : 1 was continuously demonstrated. The Faraday efficiency of HERs and OERs were both close to 100%, demonstrating that the photocurrent is all attributed to OERs and HERs.

The efficiency of the $NiO/CoO_x/BiVO_4$ photoanode was verified by measuring the wavelength dependence of incident photon conversion efficiency (IPCE), using the intensity-calibrated Xe lamp with bandpass filters. Fig. 5 shows the result. IPCE reaches 0.45 at 0.6 V_{RHE} and 420 nm, which matches the PEC photocurrent density at 0.56 V_{RHE} by supposing a constant IPCE below 420 nm and multiplying the whole absorbed solar spectrum.

The present bulky crystallite $BiVO_4$ thin film, with a superior mechanical robustness, exhibited high PEC performance and durability comparable to foregoing nanoporous and other types of O_2-evolving undoped $BiVO_4$ photoelectrodes.[12,22,23] The robustness originates from the large $BiVO_4$ grain size, which is inherited from the precursor BiO film, derived from the BiC_xO_y film deposited on ITO. The solid BiO calcination at 520 °C with diffusion of V from $VO(acac)_2$ is the key process for the uniform formation of stoichiometric scheelite monoclinic $BiVO_4$ without unbalanced agglomeration of the components. The purity and crystallinity of the light absorbing $BiVO_4$ grains are probably the reasons for the good charge carrying and separating properties. Although the specific surface area might be smaller than that of porous-type materials, the impregnated CoO_x and ALD NiO formed conformal rough surfaces, acting as a highly active cocatalyst for O_2 evolution. The advantages of impregnated CoO_x and ALD NiO cocatalysts were explained in detail in our previous report.[8]

Conclusions

We developed a new route for the synthesis of highly active, durable oxygen evolving, bulky crystalline $BiVO_4$ film photoanodes on ITO glass. After modification with impregnated CoO_x and ALD NiO, the $BiVO_4$ electrode performs with a half-cell solar-to-hydrogen energy conversion efficiency of over 1.5% as an oxygen-evolving photoanode for water splitting under solar simulator AM 1.5G illumination. The high activity is maintained for 12 h at the operation potential of 0.6 and 0.9 V_{RHE} with continuous and stoichiometric hydrogen and oxygen evolution. Mechanical strength is one of the superior properties owing to the firmly fixed $BiVO_4$ crystallites on ITO substrates. The transparent characteristic of this electrode with respect to longer wavelength light in the solar spectrum further enables its use in tandem-type stand-alone water splitting devices assembled with hydrogen-evolving photocathodes made of narrow-bandgap p-type semiconductors.

Acknowledgements

This work was financially supported by the Artificial Photosynthesis Project of the New Energy and Industrial Technology Development Organization (NEDO) and Ministry of Economy, Trade and Industry (METI). Authors thank Mrs Yoshie Nagatsuma, who enthusiastically carried out important experiments in this work.

Notes and references

1 M. Grätzel, *Nature*, 2001, **414**, 338–344.
2 S. W. Boettcher, J. M. Spurgeon, M. C. Putnam, E. L. Warren, D. B. Turner-Evans, M. D. Kelzenberg, J. R. Maiolo, H. A. Atwater and N. S. Lewis, *Science*, 2010, **327**, 185–187.
3 Z. Wang, K. Teramura, S. Hosokawa and T. Tanaka, *J. Mater. Chem. A*, 2015, **3**, 11313–11319.
4 J. Zhao, T. Minegishi, L. Zhang, M. Zhong, M. Nakabayashi, G. J. Ma, T. Hisatomi, M. Katayama, S. Ikeda, N. Shibata, T. Yamada and K. Domen, *Angew. Chem., Int. Ed.*, 2014, **53**, 11808–11812.
5 M. Zhang, M. de Respinis and H. Frei, *Nat. Chem.*, 2014, **6**, 362–367.
6 M. W. Kanan and D. G. Nocera, *Science*, 2008, **321**, 1072–1075.
7 L. Trotochaud, S. L. Young, J. K. Ranney and S. W. Boettcher, *J. Am. Chem. Soc.*, 2014, **136**, 6744–6753.
8 M. Zhong, T. Hisatomi, Y. Kuang, J. Zhao, M. Liu, A. Iwase, Q. Jia, H. Nishiyama, T. Minegishi, M. Nakabayashi, N. Shibata, R. Niishiro, C. Katayama, H. Shibano, M. Katayama, A. Kudo, T. Yamada and K. Domen, *J. Am. Chem. Soc.*, 2015, **137**, 5053–5060.
9 Y. Lin, Y. Xu, M. T. Mayer, Z. I. Simpson, G. Mcmahon, S. Zhou and D. Wang, *J. Am. Chem. Soc.*, 2012, **134**, 5508–5511.
10 F. F. Abdi, L. Han, A. H. M. Smets, M. Zeman, B. Dam and R. van de Krol, *Nat. Commun.*, 2013, **4**, 2195.
11 J. A. Seabold and K.-S. Choi, *J. Am. Chem. Soc.*, 2012, **134**, 2186–2192.
12 T. W. Kim and K.-S. Choi, *Science*, 2014, **343**, 990–994.
13 A. Ziani, E. Nurlaela, D. S. Dhawale, D. A. Silva, E. Alarousu, O. F. Mohammed and K. Takanabe, *Phys. Chem. Chem. Phys.*, 2015, **17**, 2670–2677.
14 F. F. Abdi, T. J. Savenije, M. M. May, B. Dam and R. van de Krol, *J. Phys. Chem. Lett.*, 2013, **4**, 2752–2757.
15 X. Shi, K. Zhang, J. Kwon, D. Y. Kim, J. K. Lee, S. H. Oh, J. K. Kim and J. H. Park, *Nat. Commun.*, 2014, **5**, 4775.
16 Y. Pihosh, I. Turkevych, K. Mawatari, J. Uemura, Y. Kazoe, S. Kosar, K. Makita, T. Sugaya, T. Matsui, D. Fujita, M. Tosa, M. Kondo and T. Kitamori, *Sci. Rep.*, 2015, **5**, 11141.
17 M. Zhong, Y. Li, I. Yamada and J.-J. Delaunay, *Nanoscale*, 2012, **4**, 1509–1514.
18 M. Zhong, Y. Sato, M. Kurniawan, A. Apostoluk, B. Masenelli, E. Maeda, Y. Ikuhara and J.-J. Delaunay, *Nanotechnology*, 2012, **23**, 495602.
19 D. Kang, Y. Park, J. Hill and K.-S. Choi, *J. Phys. Chem. Lett.*, 2014, **5**, 2994–2999.
20 M. Zhong, Y. Ma, P. Oleynikov, K. Domen and J.-J. Delaunay, *Energy Environ. Sci.*, 2014, **7**, 1693–1699.
21 S. Tokunaga, H. Kato and A. Kudo, *Chem. Mater.*, 2001, **13**, 4624–4628.
22 E. Alarcón-Lladó, L. Chen, M. Hettick, N. Mashouf, Y. Lin, A. Javey and J. W. Ager, *Phys. Chem. Chem. Phys.*, 2014, **16**, 1651–1657.
23 L. Chen, F. M. Toma, J. K. Cooper, A. Lyon, Y. Lin, I. D. Sharp and J. W. Ager, *ChemSusChem*, 2015, **8**, 1066–1071.
24 L. Chen, J. Yang, S. Klaus, L. J. Lee, R. Woods-Robinson, J. Ma, Y. Lum, J. K. Cooper, F. M. Toma, L. Wang, I. D. Sharp, A. T. Bell and J. W. Ager, *J. Am. Chem. Soc.*, 2015, **137**, 9595–9603.
25 A. A. Zavýalova, R. M. Imamov and Z. G. Pinsker, *Kristallografiya*, 1965, **10**, 480.
26 M. Prekajski, A. Kremenović, B. Babić, M. Rosić, B. Matović, A. Radosavljević-Mihajlović and M. Radović, *Mater. Lett.*, 2010, **64**, 2247–2250.
27 K. Hirota, G. Komatsu, M. Yamashita, H. Takemura and O. Yamaguchi, *Mater. Res. Bull.*, 1992, **27**, 823–830.

